RSC Advances

ROYAL SOCIETY OF CHEMISTRY

www.rsc.org/advances

Effect of donor doping in B sites on electrocaloric effect of $BaTi_{1-x}Nb_xO_3$ ceramics

Yang Bai[a], Xi Han and Li-Jie Qiao

Key Laboratory of Environmental Fracture (Ministry of Education), University of Science and Technology Beijing, Beijing 100083, China

Abstract. This paper demonstrates the effect of donor doping in B sites on the electrocaloric effect (ECE) in $BaTi_{1-x}Nb_xO_3$ (x=0~0.01) ferroelectric ceramics. The Nb substitution on Ti does not affect the formation of perovskite structure, while it obviously inhabits the grain growth in sintering process. The donor doping of Nb controls the ferroelectric phase transition more efficiently than the equivalent substitutions either in A or B sites. It lowers the phase transition temperature about one order of magnitude faster than the equivalent substitution, so that the ECE ΔT_{max} shifts accordingly. Nb doping also diffuses the phase transition, so that the ECE ΔT_{max} reduces and the peak becomes much wider. Compared with $BaTiO_3$, ΔT_{max} of $BaTi_{0.994}Nb_{0.006}O_3$ drops one third, while the full width at half maximum increases twice, indicating a better refrigeration capacity.

[a] Corresponding author. Email: baiy@mater.ustb.edu.cn. Fax: 86-10-62332345

1. Introduction

High performance and small size are the trends of electronic equipments, which great accelerate in recent years. However, large amount of high power devices working in a small space will induce local high temperature, which degrades the performance of electronic devices and may even lead to complete failure. Recently, ferroelectric cooling based on electrocaloric effect (ECE) is regarded as the best solution of solid-state refrigeration for miniaturized electronic products and is absorbing great attraction, due to the advantages of easy miniaturization, high efficiency and low cost. Since a giant ECE of ΔT_{max}= 12K was obtained in $PbZr_{0.95}Ti_{0.05}O_3$ thin film in 2006 [1], the researches on ECE boom in various ferroelectric ceramics [2-21].

ECE is a basic feature of ferroelectric materials and refers to a reversible change in entropy and temperature caused by the electric field-induced variation of polarization states. Similar to magnetocaloric effect, ECE is only remarkable in the very vicinity of a phase transition, so it is thought to be closely related to the feature of ferroelectric phase transition [4]. $BaTiO_3$ with typical first order phase transition (FOPT) has a sharp ECE peak near Curie temperature with a giant ECE strength $|\Delta T/\Delta E|$ [5-8]. Then many researches are devoted in material design by various substitutions to widen the temperature window. For example, the substitution of Sr^{2+} on Ba^{2+} increasingly diffuses the phase transition to reduce ΔT_{max} and widen the peak [9-11]. The substitution of Zr^{4+} on Ti^{4+} also diffuses the phase transition and results in a high ΔT in a broad temperature range [12,13]. The substitution of Sn^{4+} on Ti^{4+} leads to a

high ***ΔT*** at morphotropic phase boundary [14,15]. In addition, the co-substitution of Ca^{2+} on Ba^{2+} and Zr^{4+} on Ti^{4+} was also studied [16-21]. Up to now, all reports focused on the effect of various equivalent dopings but the inequivalent doping has not been researched for ECE, although the inequivalent dopings were reported to improve the dielectric and piezoelectric properties more efficiently [22,23]. The donor doping of Nb^{5+} on Ti^{4+} in B sites, a typical soft doping, has a notable effect on modifying the ferroelectric phase transition. This paper reports its effects on the phase composition, microstructure, dielectric, ferroelectric and electrocaloric effects of $BaTiO_3$ ceramics, and a better refrigeration capacity is obtained.

2. Experimental procedure

2.1 Sample preparation

The $BaTi_{1-x}Nb_xO_3$ (x=0~0.01) ceramics were prepared by the conventional solid-state reaction method. Analytical reagent grade $BaCO_3$, TiO_2 and Nb_2O_5 were used as raw materials. After the mixed powders were calcined at 1000 °C, they were grinded by planetary ball mill. The resultant powders were dry-pressed in a stainless-steel die under a pressure of 3 MPa and the pressed pellets were sintered at 1350 °C for 4 hours in air.

2.2 Characterization

The phase composition of calcined powders were characterized by X-ray diffraction (XRD) using Cu K_α radiation (λ=0.15418 nm) with a scanning rate of 2 °/min. The microstructure of the sintered samples was observed by scanning electron

microscope (SEM, JSM-6510A). The densities of the sintered samples were measured by Archimedes' method. The heat flow curve was measured using a differential scanning calorimeter (DSC, TA Instruments Q2000) under a heating rate of 10 °C/min. The permittivity was measured between 50 and 150 °C by an HP4192 impedance analyzer with a temperature chamber. The ferroelectric hysteresis measurements were carried out at 10 Hz using a TF2000 analyzer in the temperature range of 25~150°C.

3. Results

3.1 Phase composition

Figure 1 shows the XRD pattern of $BaTi_{1-x}Nb_xO_3$ (x= 0.001, 0.004, 0.01) powders calcined at 1000 °C. The results are carefully indexed with the standard XRD pattern (PDF 05-0626). All sample show a well-defined perovskite phase and there is no impurity phase in each sample. The lattice parameters of the calcined powders are about a=4.000~4.004Å, whose change for the samples with different Nb doping is as tiny as comparable to the instrumental error. It is because the doping amount is very small and the radius difference between Nb^{5+} (0.064nm) and Ti^{4+} (0.061nm) is very small. In addition, the XRD spectra do not show obvious tetragonal distortion, i.e. c/a≈1, due to the small particle size of powder specimens.

3.2 Microstructure

After all samples are sintered at 1350 °C for 4 hours, they exhibit dense microstructure similarly. Figure 2 (a)~(d) show the SEM photos of the microstructure for the x=0.00~0.008 samples as examples. Compared with pure $BaTiO_3$ ceramics

(Figure 2(a)), Nb doped samples exhibit obviously small grain size, less than 1μm, which further decreases with increasing Nb amount (Figure 2 (b)~(d)). It is because the donor doping of Nb accumulates at grain boundaries, which hinders the motion of grain boundaries during the sintering process. The densities of all sintered samples are larger than 5.92 g/cm^3, i.e. 98% of theoretical density, which well agrees with the SEM observations.

3.3 Thermal analysis

The thermal characters of tetragonal-cubic (T-C) phase transition are shown in the heat flow curves in Figure 3. With the rise of Nb amount, the endothermic peak gradually moves to lower temperature, indicating a linear shift of phase transition with a fitting equation of T_1=-3140x+122 (^{o}C), as shown in the upper inset of Fig. 3. The slope is much higher than that in previous reports for equivalent substitutions, such as Sr, Zr and Sn. It implies that the donor doping of Nb is more efficient for phase transition shift. In addition, the endothermic peak turns flatter and the latent heat reduces with the rise of Nb amount due to the diffusion of first order phase transition.

3.4 Temperature dependence of permittivity

Figure 4 shows the temperature dependence of permittivity for the samples with different Nb amount. The phase transition shifts to lower temperature with the rise of Nb amount and the peak value of permittivity gradually drops, which agrees with the DSC results.

The reduction of permittivity maximum at Curie temperature is related to the

diffused ferroelectric phase transition. Based on Smolenski' composition fluctuation theory and Curie-Weiss law, the diffused phase transition was characterized by diffusion exponent $\boldsymbol{\alpha}$ using the equation of

$$\frac{1}{\varepsilon_r(T)} - \frac{1}{\varepsilon_{rm}} = \frac{(T-T_m)^{\alpha}}{2\varepsilon_{rm}\sigma^2} \quad (1).$$

As shown in the inset of Figure 4, $\boldsymbol{\alpha}$ rises with increasing Nb amount, i.e. the phase transition is diffused gradually.

3.5 Ferroelectric and electrocaloric properties

The sintered $BaTi_{1-x}Nb_xO_3$ samples exhibit good ferroelectric hysteresis loops with high polarization value. And the ferroelectric hysteresis loops of all samples have similar variation trend with the rise of temperature. The P-E loop shrinks gradually and the polarization value decreases, which exhibits a sudden drop at Curie temperature. Figure 5 (a) (b) and (c) show the typical ferroelectric hysteresis loops of the x=0.002, 0.006 & 0.01 samples at different temperatures, respectively.

Based on the Maxwell relation of $(\partial \boldsymbol{P}/\partial \boldsymbol{T})_{\boldsymbol{E}}=(\partial \boldsymbol{S}/\partial \boldsymbol{E})_{\boldsymbol{T}}$, the ECE $\boldsymbol{\Delta T}$ and $\boldsymbol{\Delta S}$ is calculated as following

$$\Delta T = -\frac{1}{\rho}\int_0^E \frac{T}{C}\left(\frac{\partial P}{\partial T}\right)_E dE \quad (1),$$

$$\Delta S = -\int_0^E \left(\frac{\partial P}{\partial T}\right)_E dE \quad (2).$$

Figure 6 shows the $\boldsymbol{\Delta T}$-$\boldsymbol{T}$ curves of the x=0.006 samples as an example. There is a remarkable ECE peak in the vicinity of phase transition. The ECE $\boldsymbol{\Delta T_{max}}$ always occurs above Curie temperature, compared with the results of DSC and permittivity. With increasing electric fields, the ECE $\boldsymbol{\Delta T}$ enhances and $\boldsymbol{\Delta T_{max}}$ shifts to higher

temperatures.

Figure 7 shows the ΔT_{max} as a function of Nb amount. With the rise of Nb amount, the ECE ΔT_{max} moves to lower temperature, which is associated to the electric field-induced shift of ferroelectric phase transition. At the same time, the ECE ΔT_{max} drops gradually and the peak turns wider, which is determined by the diffusion of phase transition. This phenomenon is similar to previous reports on Sr, Zr or Sn doped $BaTiO_3$ [9-14]. Under an E=20kV/cm field, ΔT_{max} = 0.98 K (ΔS=1.24 J/kg·K) for x=0, ΔT_{max} = 0.89 K (ΔS=1.14 J/kg·K) for x=0.002 and ΔT_{max} = 0.66 K (ΔS=0.86 J/kg·K) for x=0.006, while the full width at half maxium (FWHM) of ECE peaks is 8°C, 16 °C and 24 °C, respectively. The variations of ΔT_{max} and FWHM are also shown in Figure 7.

4. Discussions

The donor doping, such as Nb^{5+}, is soft doping for ferroelectric materials and can improve the dielectric and piezoelectric properties [22,23]. It increases the dielectric permittivity and reduce the coercive force because easy polarization under external fields. The change of polarization under the couple effect of external electric field and temperature plays a key role for ECE, including ferroelectric phase transition and domain switching.

Our work shows that the donor doping of Nb is efficient to modify the ferroelectric phase transition, including shifting transition point and diffusing transition, so does the ECE. When Nb^{5+} ion with a bit larger radius (0.064nm) substitutes for Ti^{4+}

(0.061nm) ion in B site, Nb^{5+} locates at the center site of oxygen octahedrons same as Ti^{4+} but the band of Nb-O is weakened. On the other hand, the valence state of Nb^{5+} is higher than that of Ti^{4+}, which further weakens the crystalline field. In addition, some cation vacancies form at the same time which can ease the domain switching. Because the doping amount is too small ($x \leq 0.01$) to induce obvious lattice distortion, which is confirmed by the XRD results, different valence state affects the crystalline field dominantly. That is different from the effect of equivalent dopings, such as Sr^{2+} in A site and Zr^{4+} in B site, where the lattice distortion is the key. Our results show that the phase transition changes more rapid with the donor doping of Nb than the equivalent substitutions. For example, the shift of Curie temperature is about one order of magnitude faster than that of Sr substitution [9]. Each 1% Nb doping lowers T_c about 31 °C, while each 1% Sr doping only lowers T_c 3 °C. In addition, the composition fluctuation and local inhomogeneous internal stress destroy the phase transition consistency, so the phase transition is obviously diffused with Nb amount.

5. Conclusions

This paper investigated the ECE of $BaTi_{1-x}Nb_xO_3$ ceramics prepared by the solid state reaction method. The sintered Nb doped ceramics has fine-grained microstructures. Nb doping has more efficient to modify the ferroelectric phase transition. With the rise of Nb amount, the phase transition shifts to lower temperature more rapidly than that for equivalent substitutions, and the transition is diffused at the same time. As a result, the ECE ΔT_{max} reduces and shifts to lower temperature with

increasing Nb amount, and the ECE peak becomes much wider. $BaTi_{0.994}Nb_{0.006}O_3$ has ΔT_{max} = 0.66 K (@E=20kV/cm) and FWHM=24 °C, where ΔT_{max} drops one third of that in $BaTiO_3$ and FWHM increases twice, i.e. a better refrigeration capacity. This work implies that inequivalent substitution is a more efficient method to adjust the ECE in ferroelectric ceramics, which can great enrich the material design for ferroelectric refrigeration.

ACKNOWLEDGEMENT

This work was supported by grants from the National Science Foundation of China (51172020 and 51372018), the National Program for Support of Top-Notch Young Professionals, the Program for New Century Excellent Talents in University (NCET-12-0780), the Beijing Higher Education Young Elite Teacher Project (YETP0414), and the Program for Changjiang Scholars and Innovative Research Team in University (IRT1207).

Reference

[1] S. Mischenko, Q. Zhang, J. F. Scott, R. W. Whatmore and N. D. Mathur, *Science*, 2006, **311**, 1270-1271.

[2] B. Neese, B. Chu, S. G. Lu, Y. Wang, E. Furman and Q. M. Zhang, *Science*, 2008, **321**, 821-823.

[3] Y. Bai, G. P. Zheng and S. Q. Shi, *Appl. Phys. Lett.*, 2010, 96, 192902.

[4] Y. Bai, K. Ding, G. P. Zheng, S. Q. Shi and L. Qiao, *Phys. Status Solidi A*, 2012, **209**, 941-944.

[5] Y. Bai, X. Han, X. C. Zheng and L.J. Qiao, Sci. Rep., 2013, **3**, 02895.

[6] X. Moya, E. Stern-Taulats, S. Crossley, D. González-Alonso, S. Kar-Narayan, A. Planes, L. Mañosa and N. D. Mathur, *Adv. Mater.*, 2013, **25**, 1360-1365.

[7] Y. Bai, K. Ding, G. P. Zheng, S. Q. Shi, J. L. Cao and L. J. Qiao, AIP Adv., 2012, **2**, 022162.

[8] H. H. Wu, J. Zhu and T. Y. Zhang, *RSC Adv.*, 2015, **5**, 37476-37484.

[9] Y. Bai, X. Han, K. Ding and L.J. Qiao, *Appl. Phys. Lett.*, 2013, **103**, 162902.

[10] X. Q. Liu, T. T. Chen, Y. J. Wu and X. M. Chen, *J. Am. Ceram. Soc.*, 2013, **96**, 1021-1023.

[11] X. Q. Liu, T. T. Chen, M. S. Fu, Y. J. Wu and X. M. Chen, *Ceram. Int.*, 2014, **40**, 11269-11276.

[12] X. S. Qian, H. J. Ye, Y. T. Zhang, H. Gu, X. Li, C. A. Randall and Q. M. Zhang, *Adv. Funct. Mater.*, 2014, **24**, 1300-1305.

[13] H. J. Ye, X. S. Qian, D. Y. Jeong, S. J. Zhang, Y. Zhou, W. Z. Shao, L. Zhen and

Q. M. Zhang, *Appl. Phys. Lett.*, 2014, **105**, 152908.

[14] Z. Luo, D. Zhang, Y. Liu, D. Zhou, Y. Yao, C. Liu, B. Dkhil, X. Ren and X. Lou, *Appl. Phys. Lett.*, 2014, **105**, 102904.

[15] Tao Shi, Lin Xie, Lin Gu and Jing Zhu, *Sci. Rep.*, 2015, **5**, 08606.

[16] Y. Bai, X. Han and L.J. Qiao, *Appl. Phys. Lett.*, 2013, **102**, 252904.

[17] M. Sanlialp, V. V. Shvartsman, M. Acosta, B. Dkhil and D. C. Lupascu, *Appl. Phys. Lett.*, 2015, **106**, 062901.

[18] G. Singh, I. Bhaumik, S. Ganesamoorthy, R. Bhatt, A. K. Karnal V. S. Tiwari and P. K. Gupta, *Appl. Phys. Lett.*, 2013, **102**, 082902.

[19] G. Singh, V. S. Tiwari and P. K. Gupta, *Appl. Phys. Lett.*, 2013, **103**, 202903.

[20] B. Asbani, J. L. Dellis, A. Lahmar, M. Courty, M. Amjoud, Y. Gagou, K. Djellab, D. Mezzane, Z. Kutnjak and M. El Marssi, *Appl. Phys. Lett.*, 2015, **106**, 042902.

[21] J. F. Wang, T. Q. Yang, S. C. Chen, G. Li, Q. F. Zhang and X. Yao, *J. Alloy. Comp.*, 2013, **550**, 561.

[22] Dong Guo, Kai Cai, Longtu Li and Zhilun Gui, *J. Appl. Phys.*, 2009, **106**, 054104.

[23] Dong Guo, Longtu Li, Cewen Nan, Juntao Xia and Zhilun Gui, J. Euro. Ceram. Soc., 2003, **23**, 2177.

Figure captions.

Figure 1. The XRD spectra of $BaTi_{1-x}Nb_xO_3$ (x=0.001-0.01) calcined at 1000°C.

Figure 2. The microstructure of the samples (x=0.0, 0.004, 0.006 & 0.008) sintered at 1350°C.

Figure 3. Heat flow curves of $BaTi_{1-x}Nb_xO_3$ ceramics in a heating process. The inset shows the variation of Curie temperature.

Figure 4. Temperature dependence of permittivity of $BaTi_{1-x}Nb_xO_3$ ceramics. The inset show the composition dependence of $\boldsymbol{\alpha}$.

Figure 5. Ferroelectric hysteresis loops of $BaTi_{1-x}Nb_xO_3$ ceramics at different temperatures. (a) x=0.002; (b) x=0.006; (c) x=0.01.

Figure 6. Temperature dependence of ECE $\boldsymbol{\Delta T}$ of $BaTi_{1-x}Nb_xO_3$ (x=0.006) under different applied electric fields.

Figure 7. The ECE $\boldsymbol{\Delta T_{max}}$ and FWHM as a function of Nb amount (x=0~0.01).

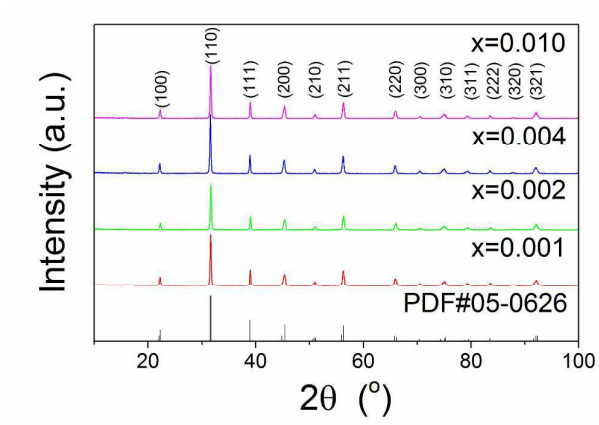

Figure 1. The XRD spectra of $BaTi_{1-x}Nb_xO_3$ (x=0.001-0.01) calcined at 1000°C.

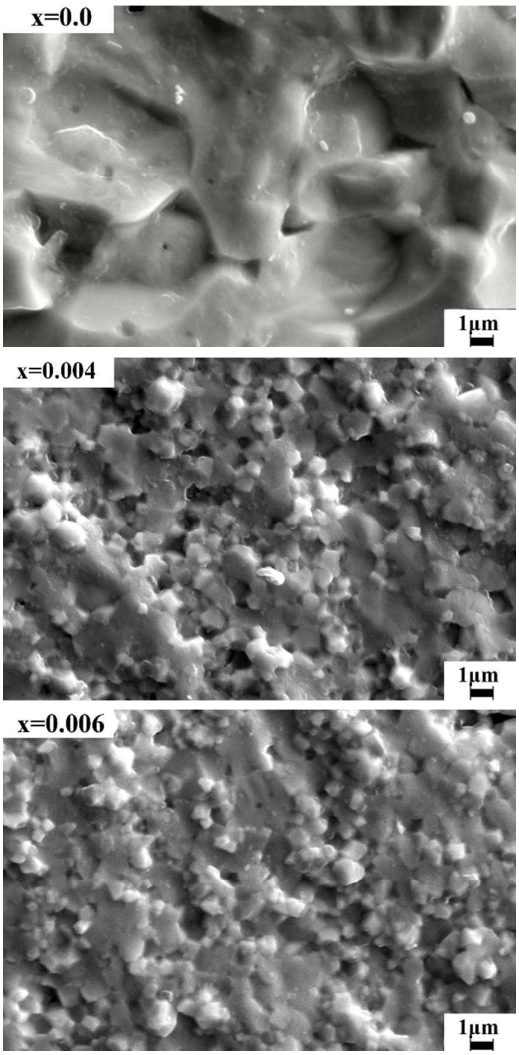

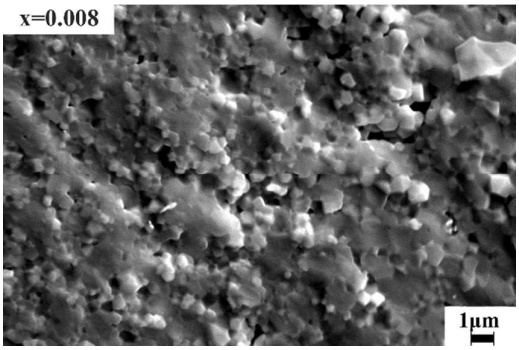

Figure 2. The microstructure of the samples (x=0.004 & 0.008) sintered at 1350°C.

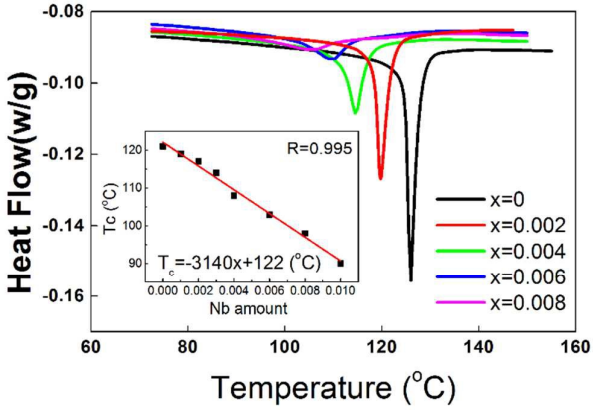

Figure 3. Heat flow curves of $BaTi_{1-x}Nb_xO_3$ ceramics in a heating process. The inset shows the variation of Curie temperature.

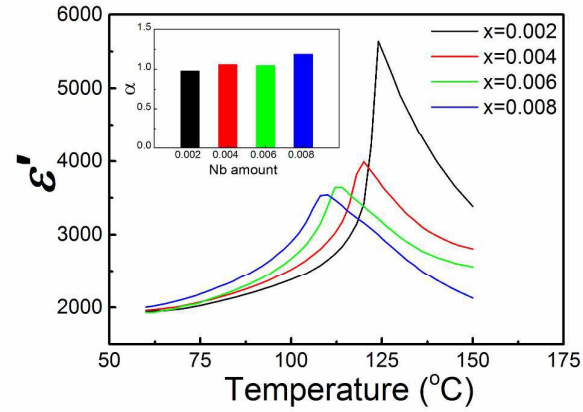

Figure 4. Temperature dependence of permittivity of $BaTi_{1-x}Nb_xO_3$ ceramics. The inset show the composition dependence of α.

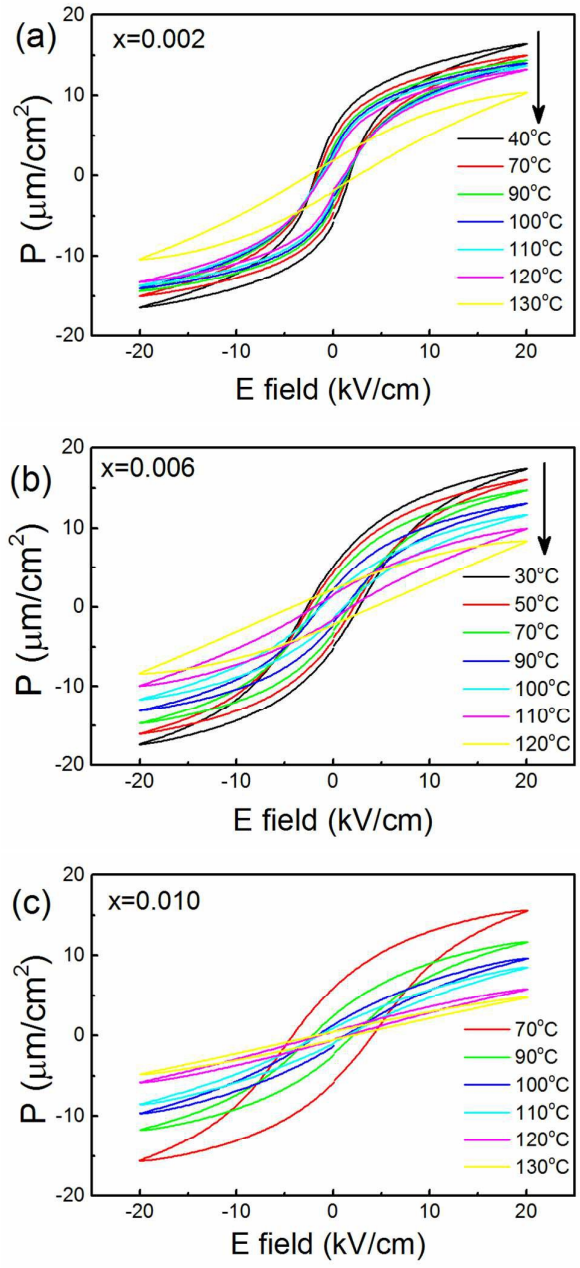

Figure 5. Ferroelectric hysteresis loops of $BaTi_{1-x}Nb_xO_3$ (x=0.006) ceramics at different temperatures.

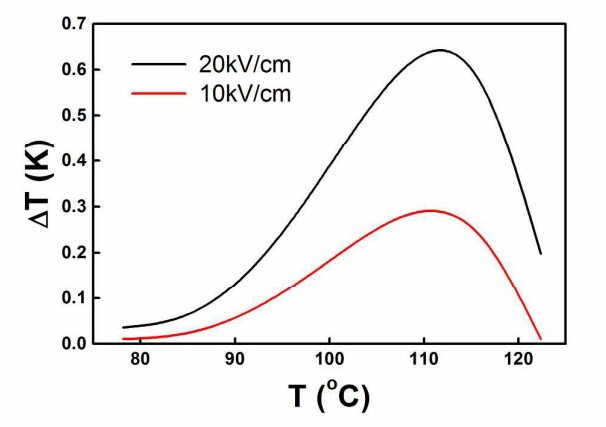

Figure 6. Temperature dependence of ECE ΔT of $BaTi_{1-x}Nb_xO_3$ (x=0.006) under different applied electric fields.

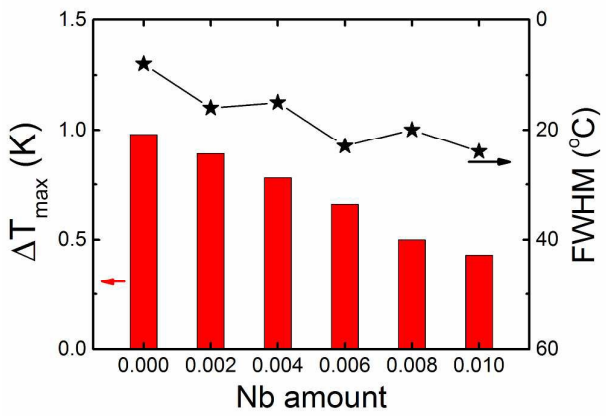

Figure 7. The ECE ΔT_{max} and FWHM as a function of Nb amount.